

NUMERICAL MODELLING OF FLOW AND COUPLED MASS AND HEAT TRANSFER IN AN ADSORPTION PROCESS

Dang CHENG*, E.A.J.F. PETERS, J.A.M. KUIPERS

Multiphase Reactors Group

Department of Chemical Engineering & Chemistry

Eindhoven University of Technology, THE NETHERLANDS

*Corresponding author, E-mail address: d.cheng@tue.nl

ABSTRACT

In this paper, a detailed 3D modelling of flow and coupled heat and mass transport in a channel coated with adsorbing material is presented. A comparative study between a simplified 1D model and the detailed 3D model is carried out. Both 3D and 1D predictions are compared with experimental data available from literature as well. The time-dependent variation of temperature and heat flux distribution at the interface between the gas channel and the adsorbent layer encourages the development and use of a more detailed 3D model.

NOMENCLATURE

A_{duct}	cross sectional area of gas duct	m^2
A_{tot}	total cross sectional area of a channel with adsorbent layer	m^2
a	half of channel height	m
b	half of channel base	m
d	half of adsorbent wall thickness	m
C_p	specific heat	$J/(kg \cdot K)$
D	mass diffusivity	m^2/s
D_H	hydraulic diameter	m
J_{nor}	peripherally average normal total heat flux of the interface	W/m^2
k	thermal conductivity	$W/(m \cdot K)$
L	channel length	m
P	pressure	Pa
P_{duct}	wetted perimeter of the cross-section	m
P_s	Saturated vapour pressure	Pa
r_c	hydraulic radius	m
t	time	s
t_{ad}	adsorption period	s
t_{de}	desorption period	s
$\bar{T}_{1,out}$	mixing cup average temperature at gas channel outlet	K
\bar{u}_g	bulk stream velocity in gas channel	m/s
u_{face}	velocity at inlet face	m/s
$\bar{w}_{1,out}$	mixing cup average pseudo weight fraction at channel outlet	kg/kg
Greek symbols		
ε	adsorbent porosity	
r_p	porous radius	m
ρ	density	kg/m^3
σ	structural void fraction	A_{duct}/A_{tot}
μ	dynamic viscosity	$Pa \cdot s$
τ	tortuosity	

δ equivalent adsorbent layer thickness m

ϕ_w relative humidity

Subscripts and superscripts

a	dry gas
f	entire adsorbent material (matrix and pores)
fp	pores (inter-particle voids)
fm	matrix part of the adsorbent material (solid part, adsorbed adsorbate, but excluding pores)
fs	dry solid adsorbent material (exclude pores and adsorbed adsorbate)
g	process stream air
M	molecular
l	adsorbed liquid
v	sorbate vapour
eff	effective property
in, out	inlet / outlet of the gas channel
s	solid

INTRODUCTION

Open gas channels coated with adsorbent layers are applied in many industrial processes. One example of such a process is the removal of volatile components from air streams. When operated in an adsorption mode, the sorbate-vapour present in the process gas stream is adsorbed in the coating. Commonly, a significant amount of heat is released when adsorption takes place. During the regeneration stage a hot gas stream is used with preferably a low amount of sorbate. Locally heat is consumed at desorption.

The equilibrium between vapour and the amount of material adsorbed is determined by an adsorption isotherm. This isotherm is typically temperature dependent. Since adsorption and desorption have large heat effects the temperature in a channel can vary significantly in time and space. So, during adsorption and desorption processes equilibria are 'on the move'. The level of non-equilibrium determines the mass and heat fluxes. Therefore, within these processes there is an intimate coupling of heat and mass transfer.

Considerable effort has been devoted to research and development of adsorption processes by means of both experiments and numerical modelling. The use of experiments to evaluate the importance of various parameters in such a process is a difficult, time-intensive and costly task. For example, determining the optimal

operating parameters of an adsorbing material, requires a series of experiments operating over a wide range of process conditions such as inlet concentrations, temperatures and switching schedules (between adsorption and regeneration). Clearly, for an actual process, this experimental optimization procedure would be very expensive and require constant monitoring. On the other hand, there still lacks a detailed understanding of the relevant heat and mass transport processes at play due to the fact that these processes are intrinsically highly coupled. With the development of computer hardware and numerical methodology, detailed mathematical models for parametric studies provide a viable alternative.

A large number of numerical studies were carried out to predict the adsorption in coated gas channels. However, the majority of them (Ge et al., 2008) employed one-dimensional models with axial dependence only, using overall transfer coefficients to account for the transfer rates at the interface, in which the heat and mass transfer phenomena within the porous adsorbent are not described locally in a detailed way. Only a few studies (Spaier and Worek, 2004; Ruivo et al., 2007) have attempted to take into account the local thermal and mass diffusion in the desiccant by considering a two-dimensional porous medium.

One of the difficulties in numerical simulation is the accurate representation of the solid-fluid interface transfer, which is characterized by the use of Nusselt (Nu) and Sherwood number (Sh) in the one dimensional (1D) model approach. The used Nusselt number is usually based on either a constant and uniform temperature wall boundary conditions (Nu_T) or a constant heat flux wall boundary conditions (Nu_H). However, it should be noted that the interface between the air channel and the adsorbent layer is neither constant temperature nor constant heat flux in practical systems. Hence, the use of such a Nu -correlation may reduce the reliability of 1D model approach.

For the complex corrugated channels, even for constant temperature or heat-flux boundary conditions, the Nu numbers might not have been documented in the literature and are sometimes difficult to obtain. Concerning convective heat transfer, additional work has to be carried out to obtain values of the Nusselt number in complex-shaped ducts by experiments or by detailed numerical simulation. Moreover, another related obvious disadvantage is that the 1D model is incapable of discriminating different geometries, which reduces its functionality when it comes to geometrical optimization.

Advancements in computer technology allow for the employment of more detailed, and thus more complicated, mathematical formulations. Therefore, the detailed three dimensional (3D) numerical modelling of adsorption processes is of great relevance for the geometry and system optimization by means of performing exhaustive parametric studies. Furthermore, a detailed 3D model is also a powerful tool to evaluate the range of validity of more simplified models. It is particularly noted that detailed 3D modelling that takes into account the local heat and mass transfer in a coated gas channel is still lacking in the open literature, in spite of its great importance.

The purpose of this work is to model the heat and mass transport in such a adsorbent coated air channel in a detailed way. In this paper, first a detailed 3D model and a simplified 1D model for the heat and mass transport are presented. A comparative study between the simplified 1D

model and the detailed 3D model is then described. Both model results are compared with experimental data as well. In order to get insights into the interface between the solid adsorbent and the gas channel, the temperature and heat flux distribution at the interface is finally examined.

MODEL DESCRIPTION

The following assumptions implicitly involved in this study deserve to be specifically mentioned:

1) No chemical reaction takes place, nor is there any energy sources within the system; No phase change, other than that related to the adsorption process, occurs in the exchanger.

2) Radiation effects are neglected because of the relatively low temperature in the system.

3) Body forces, such as gravity, centrifugal, Coriolis, and electromagnetic are neglected.

4) The flow in the gas channel is considered incompressible and laminar; the velocity distribution of the gas is assumed to be independent of the fluid temperature.

5) All sorption phenomena are thermodynamically reversible.

6) The specific heat and thermal conductivities of dry sorbent and liquid sorbate are assumed constant.

7) Heat and mass transfer from the surroundings to the channel are negligible.

8) The porous medium is assumed to be homogeneous and isotropic.

These simplifications are similar to those described in the previous literature. A more detailed analysis of the implications of the above idealizations was given by Spaier and Worek, (2004).

3D Governing Equations for Transport Phenomena

The three dimensional flow in this case is assumed to be incompressible or constant density, which means the flow is independent of the unsteady heat and mass transfer problem, so all unsteady terms in the continuity and momentum equations can be neglected. The continuity and momentum equations are given by the stationary, incompressible Navier-Stokes equations,

$$\nabla \cdot \mathbf{u} = 0 \quad (1)$$

$$\rho \mathbf{u} \cdot \nabla \mathbf{u} = \nabla \cdot \left[-P\mathbf{I} + \mu(\nabla \mathbf{u} + (\nabla \mathbf{u})^T) \right] \quad (2)$$

where ρ is the density, \mathbf{u} is the flow vector, P is the pressure, μ is the dynamic viscosity.

Based on the above assumptions, the mass and energy governing equations in the air channel and the adsorbent layer is modelled as follows. These model equations are fully three-dimensional.

The mass conservation of the sorbate vapour in the gas channel is formulated as:

$$\frac{\partial w_1}{\partial t} + \mathbf{u} \cdot \nabla w_1 = \nabla \cdot (D_M \nabla w_1), \quad (3)$$

where w_1 describes the density of the sorbate relative to that of the remaining components in the gas mixture, D_M is molecular diffusivity.

The energy transport equation in the gas channel is described as:

$$\rho_g C_{p,g} \frac{\partial T_1}{\partial t} + \rho_g C_{p,g} \mathbf{u} \cdot \nabla T_1 = \nabla \cdot (k_g \nabla T_1) \quad (4)$$

where $\rho_g = \rho_a(1+w_1)$ is the gas density, T_1 the temperature in the gas channel, $C_{p,g}$ the specific heat and k_g the thermal

conductivity. They are all estimated from the mass average of the clean gas and the sorbate vapour

$$C_{p,g} = \frac{\rho_a C_{p,a} + w_1 \rho_s C_{p,v}}{\rho_g} \quad (5)$$

$$k_g = \frac{\rho_a k_a + \rho_s w_1 k_v}{\rho_g} \quad (6)$$

The mass transport in the adsorbent layer is written as:

$$\varepsilon \rho_a \frac{\partial w_2}{\partial t} + \rho_{fs} f_s (1-\varepsilon) \frac{\partial W}{\partial t} = \rho_a \nabla \cdot (D_{g,eff} \nabla w_2) + \rho_{fs} f_s \nabla \cdot (D_{s,eff} \nabla W) \quad (7)$$

where ε is the porosity of the adsorbent layer, w_2 the pseudo weight fraction in the porous medium and W is the uptake describing the mass of the adsorbed liquid relative to the mass of the dry adsorbent. W and w_2 are related by a temperature dependent adsorption isotherm.

Usually the adsorbent material consists of both adsorbent and inert supporting materials, so a quantity representing the mass fraction of adsorbent in the porous desiccant layer is defined as f_s . The density of dry solid adsorbent material is designated as ρ_{fs} .

The gas diffusion in the porous adsorbent is a combination of ordinary molecular diffusion and Knudsen diffusion (Youngquist, 1970):

$$\frac{1}{D_g} = \frac{1}{D_M} + \frac{1}{D_K} \quad (8)$$

The molecular and Knudsen diffusion for mixture of air and water vapour are defined below (Ruthven, 1984):

$$D_M = 1.735 \times 10^{-9} \frac{T^{1.685}}{P} \quad (9)$$

$$D_K = 97 v_t \sqrt{\frac{T}{18.015}} \quad (10)$$

where P should be entered in atmosphere, T in Kelvin.

The surface diffusivity is calculated by using the following equation proposed in Sladek et al. (1974):

$$D_s = 1.6 \times 10^{-6} \exp\left(-0.45 \frac{i_{sor}}{RT}\right) \quad (11)$$

Effective gas diffusivity and surface diffusivity are defined as:

$$D_{g,eff} = \frac{\varepsilon D_g}{\tau_g} \quad (12)$$

$$D_{s,eff} = \frac{(1-\varepsilon) D_s}{\tau_s} \quad (13)$$

The energy transport in the adsorbent layer is given by:

$$\rho_f C_{p,f} \frac{\partial T_2}{\partial t} = \nabla \cdot (k_{f,eff} \nabla T_2) + \rho_{fs} f_s \left((1-\varepsilon) \frac{\partial W}{\partial t} - \nabla \cdot (D_{s,eff} \nabla W) \right) i_{sor} \quad (14)$$

where T_2 is the temperature of the adsorbent layer, ρ_f the density of the entire adsorbent layer, $C_{p,f}$ the specific heat of the desiccant layer, $k_{f,eff}$ is the effective thermal conductivity of the adsorbent layer and i_{sor} is heat of adsorption.

In second term on the right hand side of equation (14) is the accumulation term minus the diffusion term representing the local sorbate uptake per unit time and unit volume. Multiplying this uptake by the heat of adsorption gives the heat effect caused by vapour adsorption.

There are many components in the porous adsorbent layer including the solid matrix of the porous medium, pores, gaseous mixture (dry air plus sorbate vapour) and water uptake. It is worthwhile to note that a lot of quantities/variables should be clearly defined in order to

avoid confusion and to facilitate the numerical analysis. The density of the gas mixture in the pores is defined as ρ_{fp} , and the density of solid matrix part of the adsorbent layer is defined as ρ_{fm} . The density of adsorbent layer is derived as:

$$\rho_f = \varepsilon \rho_{fp} + (1-\varepsilon) \rho_{fm} \quad (15)$$

where

$$\rho_{fp} = \rho_a (1 + w_2) \quad (16)$$

$$\rho_{fm} = \rho_{fs} (1 + f_s W) \quad (17)$$

Similarly, the specific heat and thermal conductivity in the pores are defined as $C_{p,fp}$ and k_{fp} respectively. The corresponding specific heat and thermal conductivity of the solid matrix part of the adsorbent layer are defined as $C_{p,fm}$ and k_{fm} respectively.

The effective thermal conductivity and specific heat of the adsorbent layer are given by the following equations:

$$C_{p,fp} = \frac{\rho_a C_{p,a} + w_2 \rho_s C_{p,v}}{\rho_{fp}} \quad (18)$$

$$C_{p,fm} = \frac{\rho_{fs} C_{p,fs} + \rho_{fs} f_s W C_{p,l}}{\rho_{fm}} \quad (19)$$

$$C_{p,f} = \frac{(1-\varepsilon) \rho_{fm} C_{p,fm} + \varepsilon \rho_{fp} C_{p,fp}}{\rho_f} \quad (20)$$

$$k_{fm} = \frac{\rho_{fs} k_{fs} + \rho_{fs} f_s W k_l}{\rho_{fm}} \quad (21)$$

$$k_{fp} = \frac{\rho_a k_a + \rho_s w_2 k_v}{\rho_{fp}} \quad (22)$$

$$k_{f,eff} = \frac{(1-\varepsilon) \rho_{fm} k_{fm} + \varepsilon \rho_{fp} k_{fp}}{\rho_f} \quad (23)$$

From the above equations, we can see that the adsorbent layer is modelled in a detailed way, by taking into account simultaneously the local heat and mass transfer phenomena. Only sorbate vapour adsorption is considered in conjunction with heat and mass diffusion. Two phases co-exist in equilibrium inside the adsorbent porous medium, the equilibrium being characterized by adsorption isotherms without hysteresis.

1D Governing Equations for Transport Phenomena

The 1D mass and energy balance equations for the gas channel and the adsorbent layer are derived as well. A bulk averaged air flow velocity \bar{u}_g is assumed in the gas channel. The 1D channel structure is schematically represented in Figure 1.

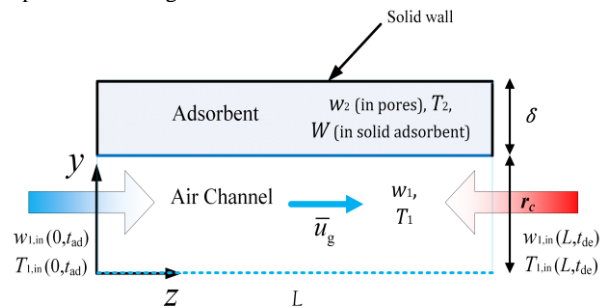


Figure 1: 1D channel with time dependent boundary conditions.

Mass transport in the air channel:

$$\frac{\partial w_1}{\partial t} + \bar{u}_g \frac{\partial w_1}{\partial z} = -\frac{4h_m}{D_H}(w_1 - w_2) \quad (24)$$

where h_m is a mass transfer coefficient. The second term on the left hand side is the adsorbate influx by fluid flow, and the right hand side models the adsorbate transfer to the adsorbent layer.

Mass transport in the adsorbent layer:

$$\begin{aligned} \varepsilon \rho_a \frac{\partial w_2}{\partial t} + \rho_{fs} f_s (1-\varepsilon) \frac{\partial W}{\partial t} &= \rho_a \frac{\partial}{\partial z} \left(D_{g,\text{eff}} \frac{\partial w_2}{\partial z} \right) \\ + \rho_{fs} f_s \frac{\partial}{\partial z} \left(D_{s,\text{eff}} \frac{\partial W}{\partial z} \right) &+ \frac{4\sigma h_m}{D_H (1-\sigma)} \rho_a (w_1 - w_2) \end{aligned} \quad (25)$$

where σ is structural void fraction of the gas channel.

Energy transport in the gas channel:

$$\rho_g C_{p,g} \frac{\partial T_1}{\partial t} + \bar{u}_g \rho_g C_{p,g} \frac{\partial T_1}{\partial z} = -\frac{4h_h}{D_H}(T_1 - T_2) \quad (26)$$

where h_h is a heat transfer coefficient. The second term on the left hand side signifies energy transferred by fluid flow, and the right hand side denotes heat transfer to the adsorbent layer.

Energy transport in the adsorbent layer:

$$\begin{aligned} \rho_t C_{p,t} \frac{\partial T_2}{\partial t} &= \frac{\partial}{\partial z} \left(k_{t,\text{eff}} \frac{\partial T_2}{\partial z} \right) + \frac{4\sigma h_h}{D_H (1-\sigma)} (T_1 - T_2) \\ + \rho_{fs} f_s \left[(1-\varepsilon) \frac{\partial W}{\partial t} - \frac{\partial}{\partial z} \left(D_{s,\text{eff}} \frac{\partial W}{\partial z} \right) \right] & i_{\text{sor}} \end{aligned} \quad (27)$$

where the third term in the right hand side is the heat effect by adsorption.

The Sh is assumed to be equal to Nu based on the analogy between mass and heat transfer:

$$Sh = Nu \quad (28)$$

The convective mass transfer coefficient is estimated as:

$$h_m = \frac{Sh \times D_M}{D_H} \quad (29)$$

The convective heat transfer coefficient is estimated as:

$$h_h = \frac{Nu \times k_g}{D_H} \quad (30)$$

Initial and Boundary Conditions

The inlet boundary condition of the air channel alternates between the process and regeneration inlet states, therefore the inlet and outlet boundary conditions of the air channel are cyclically changed. Accordingly, the air flow direction is cyclically reversed as well.

(1). Initial conditions: The temperature and humidity ratio in the adsorbent layer and air channel are assumed as uniformly distributed in their respective domain at $t=0$ s:

$$\begin{aligned} w_1 = w_2 = W &= 0 \\ T_1 = T_2 &= 293.15 \text{ K} \end{aligned}$$

In the computations, the initial conditions of each new period are the final results of the previous period.

(2). Inlet air stream conditions: The uniform and constant distributions of \mathbf{u} , T_1 and w_1 are imposed at the inlet.

For the adsorption period:

$$\begin{aligned} \mathbf{u}_{\text{in}}(0, t_{\text{ad}}) &= \mathbf{u}_{\text{inlet}} \\ w_{1,\text{in}}(0, t_{\text{ad}}) &= w_{1,\text{inlet}} \\ T_{1,\text{in}}(0, t_{\text{ad}}) &= T_{1,\text{inlet}} \end{aligned}$$

For the desorption period:

$$\begin{aligned} \mathbf{u}_{\text{in}}(L, t_{\text{de}}) &= -\mathbf{u}_{\text{inlet}} \\ w_{1,\text{in}}(L, t_{\text{de}}) &= w_{1,\text{inlet}} \\ T_{1,\text{in}}(L, t_{\text{de}}) &= T_{1,\text{inlet}} \end{aligned}$$

(3). Outlet gas stream conditions: Ambient pressure is used as the velocity field outlet conditions.

$$\left[-PI + \mu (\nabla \mathbf{u} + (\nabla \mathbf{u})^T) \right] \mathbf{n} = -\bar{p}_0 \mathbf{n}$$

Zero normal gradients are specified for all other variables at the outlet boundary:

$$\begin{aligned} -\mathbf{n} \cdot D_M \nabla w_1 &= 0 \\ -\mathbf{n} \cdot (-k_g \nabla T_1) &= 0 \end{aligned}$$

(4). Interface conditions: Boundary conditions at the solid-fluid interface are derived through mass and energy balances:

$$\begin{aligned} -\rho_a D_{g,\text{eff}} \frac{\partial w_2}{\partial \mathbf{n}} &= -\rho_a D_M \frac{\partial w_1}{\partial \mathbf{n}} \\ -k_{t,\text{eff}} \frac{\partial T_2}{\partial \mathbf{n}} &= -k_g \frac{\partial T_1}{\partial \mathbf{n}} - \rho_{fs} f_s D_{s,\text{eff}} i_{\text{sor}} \frac{\partial W}{\partial \mathbf{n}} \end{aligned}$$

The no-slip condition is imposed for the flow field calculation.

(5). Wall boundary conditions: Zero flux is used as boundary condition for the solid walls.

To solve the equation systems, the finite element based solver COMSOL Multiphysics 4.4 is applied. The MATLAB in-house code (based on the LiveLink for MATLAB) is developed to handle the time-dependent boundary conditions.

RESULTS

As an example, 3D and 1D simulations are compared with the experimental data reported by Brillhart (1997), which were obtained from measurements of water adsorption and desorption in channels consisting of corrugated paper coated with sorbent material. The shape of a single channel in this sample can be represented by a sine-curved top and a flat base as shown in Figure 2.

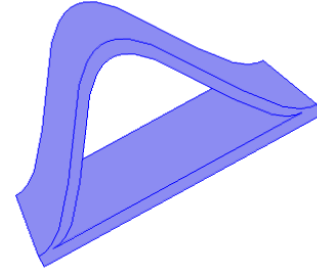


Figure 2: 3D sine tube single channel structure.

The experiments are operated in a counter-flow arrangement. The dimensions of the tube is characterized by three parameters: channel base ($2b$), channel height ($2a$) and channel wall thickness ($2d$). It should be noted that there are considerable deviations in size among the channels of the sample, and the representative values for $2b$, $2a$ and $2d$ are obtained from Spaier and Worek (2004). Two typical Nusselt numbers for the sine tubes with $a/b = 0.5$ are as follows (Shah and London, 1978): $Nu_T = 2.12$ (Constant and uniform temperature distribution at the wall), $Nu_H = 0.9$ (Constant and uniform heat flux distribution at the wall). The relevant input data including material properties and geometry are listed in Table 1.

Table 1. Input data used in the simulations

Common input data

$C_{p,a}$	1007 J/(kg·K)
$C_{p,v}$	1872 J/(kg·K)
$C_{p,l}$	4180 J/(kg·K)
k_a	0.0263 W/(m·K)
k_v	0.0196 W/(m·K)
k_l	0.613 W/(m·K)

ρ_a	1.1614 kg/m ³
ν_r	5.0×10^{-7} m
ε	0.3
τ_g	3.0
τ_s	3.0
f_s	0.8

Literature experimental validation input data

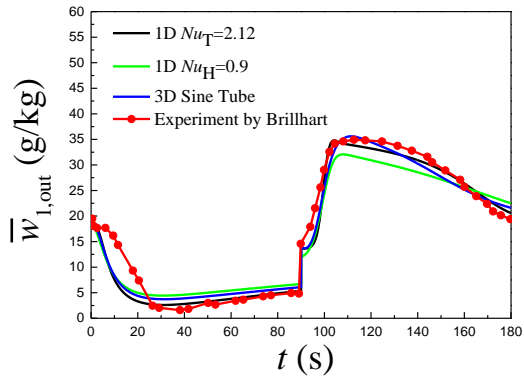
ρ_{fs}	930 kg/m ³
k_{fs}	0.011 W/(m·K)
$C_{p,fs}$	1340 J/(kg·K)
L	202.3 mm
$2a$	1.5 mm
$2b$	3.0 mm
$2d$	0.25 mm
P	1 atm
u_{face}	1.5 m/s

The adsorption isotherm for the desiccant material used in the experiments of Brillhart (2007) is given by:

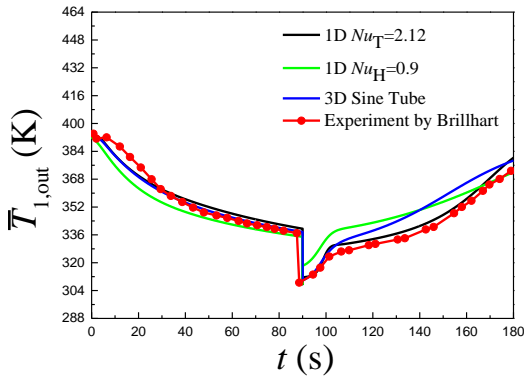
$$\begin{cases} \phi_w = (3.4188 \times W)^{1.3369} \\ P_s = \exp(23.196 - 3816.44 / (T_2 - 46.13)) \\ w_2 = \frac{0.622 \phi_w P_s}{P - \phi_w P_s} \end{cases}$$

The heat of adsorption of the test sample were actually unavailable in Brillhart (1997). The heat of adsorption was thus estimated by using the following expression (Pesaran and Mills, 1987):

$$i_{sor} = \begin{cases} -13400W + 3500 & W \leq 0.05 \\ -14000W + 2950 & W > 0.05 \end{cases}$$



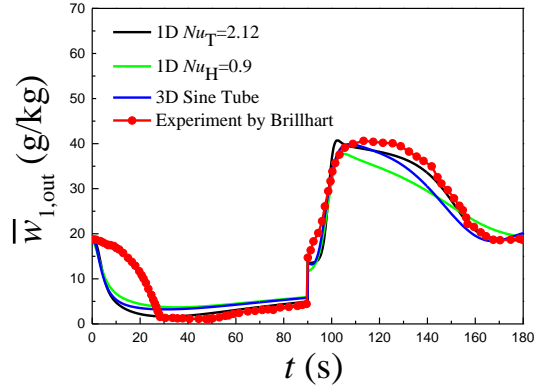
(a) Concentration variation with time.



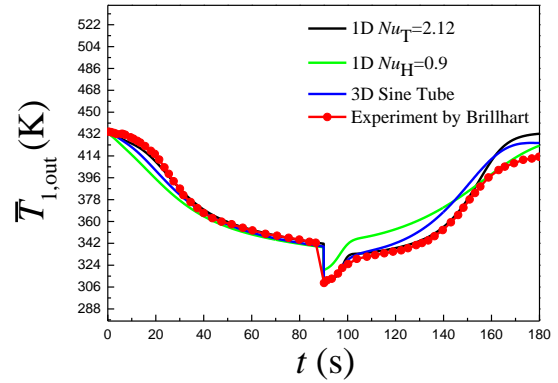
(b) Temperature variation with time.

Figure 3: Experimental validation: Outlet values of concentration and temperature with time.

$w_{1,in}(0, t_{ad})=14.5 \times 10^{-3}$, $w_{1,in}(L, t_{de})=18.5 \times 10^{-3}$ kg/kg,
 $T_{1,in}(0, t_{ad})=307.65$ K, $T_{1,in}(L, t_{de})=393.15$ K.



(a) Concentration variation with time.



(b) Temperature variation with time.

Figure 4: Experimental validation: Outlet values of concentration and temperature with time.

$w_{1,in}(0, t_{ad})=14.5 \times 10^{-3}$, $w_{1,in}(L, t_{de})=18.5 \times 10^{-3}$ kg/kg,
 $T_{1,in}(0, t_{ad})=307.65$ K, $T_{1,in}(L, t_{de})=433.15$ K.

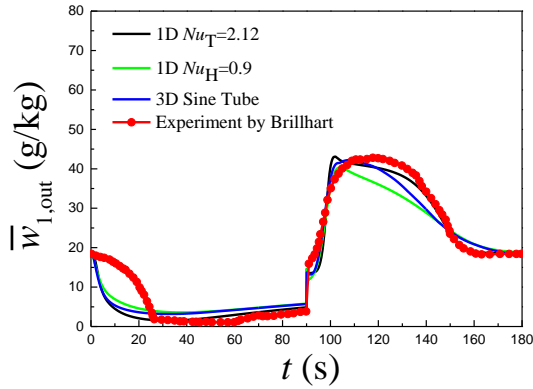
The temperature and pseudo weight fraction profiles obtained with the current 3D and 1D models are compared with those measured by Brillhart (1997) as shown in Figure 3.

As shown in Figures 4a and 4b, the results of 0~90 s are from the adsorption period, and the results of 90~180 s are from the desorption period. As the channel cyclically alternates between the process air and the regeneration air, the initial conditions of each new period are thus the final results of the previous period. Note that the humidity and temperature of the regeneration air is larger than those of the process air. When the adsorption period begins, the outlet moisture concentration equals to the concentration of the regeneration air. As the adsorbent layer adsorbs the moisture, outgoing air is dried when exits the channel, which quickly dilutes the moisture concentration. After the adsorbent layer becomes saturated, the moisture can't be adsorbed any more, then the moisture concentration starts to gradually increase until the end of the adsorption period.

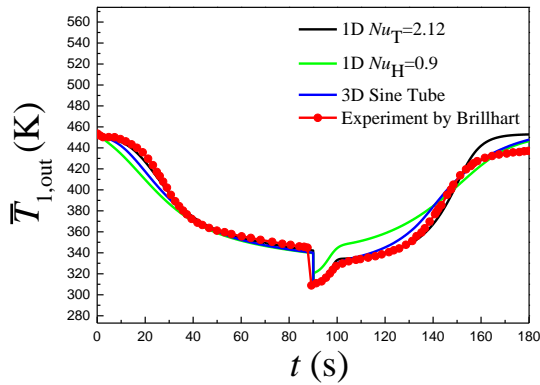
Because of the temperature of the process air is far below that of the regeneration air, so the outlet temperature continuously decreases despite the heat of adsorption that is released.

In the desorption period, hot regeneration air quickly reactivates the adsorbent layer by releasing the water uptake as it is passing through the air channel, which causes the moisture concentration to increase sharply. After the water uptake is released the outlet moisture concentration decreases again.

The temperature of the regeneration is far higher than that of the process air, the temperature continuously rises although the reactivation consumes heat energy.



(a) Concentration variation with time.



(b) Temperature variation with time.

Figure 5: Experimental validation: Outlet values of concentration and temperature with time.

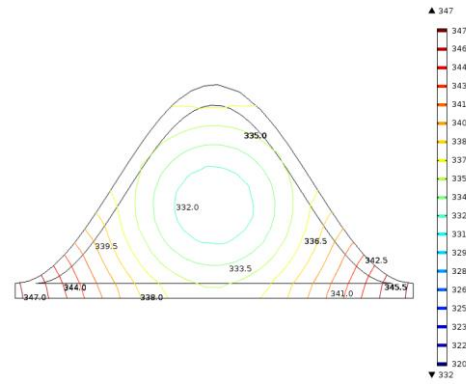
$$w_{1,\text{in}}(0, t_{\text{ad}})=14.5 \times 10^{-3}, w_{1,\text{in}}(L, t_{\text{de}})=18.5 \times 10^{-3} \text{ kg/kg},$$

$$T_{1,\text{in}}(0, t_{\text{ad}})=307.65 \text{ K}, T_{1,\text{in}}(L, t_{\text{de}})=453.15 \text{ K}.$$

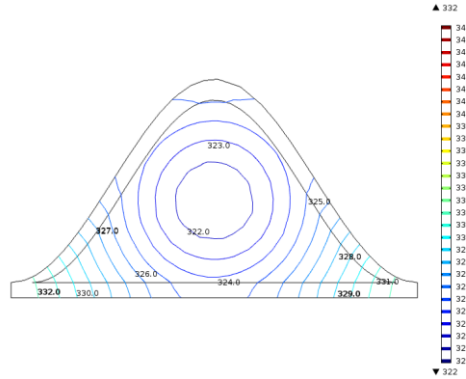
It can be seen that the 1D model results are dependent on the values of Nu , and obviously better agreement is reached by using $Nu_T=2.12$. The comparisons worsens when using $Nu_H=0.9$ in the 1D model predictions. However, it should be noted that the interface between air channel and the adsorbent layer is neither constant temperature nor constant heat flux in practical tubes. In this sense, the mass and heat transfer across the interface is not theoretically sound in the 1D model.

Overall, the 3D predictions correspond reasonably well to the respective experimental data despite the fact that only one single channel is taken into account. According to Spaier and Worek (2004), the experimental uncertainties are always largest in the beginning of an adsorption period, which thereby can justify the high discrepancy obtained in that portion of the cycle. The deviations of temperature in desorption period in Figures 3(b) and 4(b) might possibly originate from the inaccurate model used for the heat of adsorption.

In order to get insights into the interface between the solid desiccant layer and the air stream, the temperature distribution in the cross section plane at $z=L/2$ is shown in Figure 6. It can be observed that the temperature varies along the interface, which illustrates that the use of Nu_T in the 1D model is not well founded.



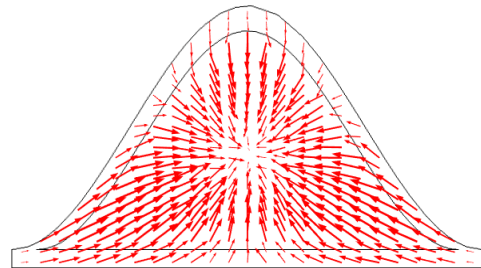
(a) $t=45 \text{ s}$



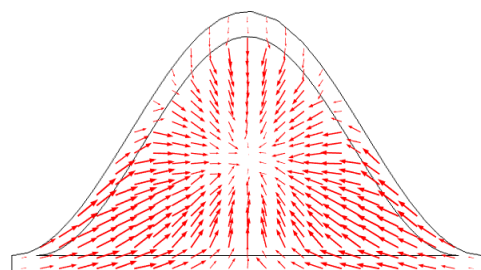
(b) $t=90 \text{ s}$

Figure 6: Temperature contour plot of cross section plane at $z=L/2$.

The heat flux distribution in the cross sectional plane at $z=L/2$ is shown in Figure 7. It can be observed that the heat flux varies along the interface as well, which actually disfavours the use of Nu_H in the 1D model.



(a) $t=45 \text{ s}$



(b) $t=90 \text{ s}$

Figure 7: Heat flux vector plot of cross section plane at $z=L/2$.

The peripherally averaged, but axially local, normal total heat fluxes of the interface along the channel length at various times are investigated as shown in Figure 8. It is evident that the normal total heat flux varies both with

time and axial location, which further discourages the use of Nu_H in the 1D model.

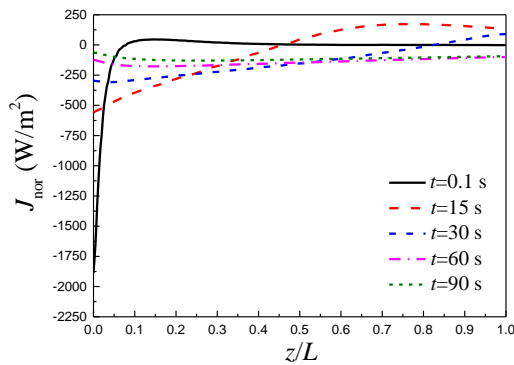


Figure 8: Peripherally average normal total heat flux of the interface along the channel length at various times.

The time-dependent variation of temperature and heat flux distribution at the interface between air channel and the adsorbent layer undermines the basis to use Nu_T and Nu_H in the 1D model, and encourages development and use of more detailed 3D model for the simulation adsorption in coated gas channels.

CONCLUSION

A detailed model is formulated that targets the numerical prediction of the transient heat and mass transport phenomena taking place in a 3D channel of a gas channel coated with adsorbent material.

The present 3D model is compared with 1D results and literature experimental data for the example of water vapour sorption. This comparative analysis showed that the 1D results are dependent on the values of Nusselt numbers, and a reasonably good agreement for 3D predictions is observed. The time-dependent variation of temperature and heat flux distribution at the interface between air channel and the adsorbent layer undermines the basis to use Nu_T and Nu_H in the 1D model in such applications, and thus encourages development and use of more detailed 3D models for the simulation of adsorption and desorption in coated gas channels. The differences between 1D and 3D simulations are expected to be much more pronounced in cases where the transport resistances are more dominating than in the current example. Therefore, 3D modeling will be essential to obtain predictive results.

REFERENCES

- BRILLHART, P.L., (1997), "Evaluation of desiccant rotor matrices using an advanced fixed-bed test system", Ph.D. thesis, University of Illinois at Chicago, Chicago, IL, USA.
- GE, T.S., Li, Y., Wang, R.Z., Dai, Y.J., (2008), "A review of the mathematical models for predicting rotary desiccant wheel", *Renew. Sustainable Energy Rev.*, 12, 1485-1528.
- PESARAN, A., (1983), "Moisture transport in silica gel particle beds", Ph.D. thesis, University of California, Los Angeles.
- RUTHVEN, D.M., (1984), "Principles of adsorption and desorption process", John Wiley & Sons, New York.
- RUIVO, C.R., COSTA, J.J., Figueiredo, A.R., (2007), "On the behaviour of hygroscopic wheels: Part 1- channel modelling", *Int. J. Heat Mass Transfer*, 50, 4813-4822.

SHAH, R.K., LONDON, A.L., (1978), "Laminar flow forced convection in ducts: A Source book for compact heat exchanger analytical data", Academic press.

SHERONY, D.F. and SOLBRIG, C.W., (1970), "Analytical investigation of heat or mass transfer and friction factors in a corrugated duct heat or mass exchanger", *Int. J. Heat Mass Transfer*, 13, 145-159.

SLADEK, J.K., GILLILAND, E.R., BADDOUR, R.F., (1974), "Diffusion on surfaces: Correlation of diffusivities of physically and chemically adsorbed species", *Ind. Eng. Chem. Fund.*, 13, 100-105.

SPHAIER, L.A and WORECK, W.M., (2004), "Analysis of heat and mass transfer in porous sorbents used in rotary regenerators", *Int. J. Heat Mass Transfer*, 47, 3415-3430.

YOUNGQUIST, G.R., (1970), "Diffusion and flow of gases in porous solids", *Ind. Eng. Chem.*, 62, 52-63.